



Contents lists available at ScienceDirect

Drug Resistance Updates

journal homepage: www.elsevier.com/locate/drup

Cell membrane-camouflaged bufalin targets NOD2 and overcomes multidrug resistance in pancreatic cancer

Wei Zhang^{a,b,c}, Yibao Fan^{a,d}, Jinze Zhang^a, Dan Shi^a, Jiahui Yuan^a, Milad Ashrafizadeh^a, Wei Li^e, Man Hu^f, A.M. Abd El-Aty^{g,h}, Ahmet Hacimuftuoglu^h, Michael Linnebacherⁱ, Yongxian Cheng^d, Weiguang Li^{j,*}, Shuo Fang^{k,*}, Peng Gong^{a,c,**}, Xianbin Zhang^{a,c,**}

^a Department of General Surgery and Institute of Precision Diagnosis and Treatment of Digestive System Tumors, Carson International Cancer Center, Shenzhen University General Hospital, Shenzhen University, Shenzhen, Guangdong 518055, China

^b Guangdong Key Laboratory for Biomedical Measurements and Ultrasound Imaging, National-Regional Key Technology Engineering Laboratory for Medical Ultrasound, School of Biomedical Engineering, Shenzhen University Medical School, Shenzhen, Guangdong 518060, China

^c International Association for Diagnosis and Treatment of Cancer, Shenzhen, Guangdong 518055, China

^d School of Pharmacy, Shenzhen University Medical School, Shenzhen University, Shenzhen, Guangdong 518060, China

^e College of Pharmacy, Shandong University of Traditional Chinese Medicine, Jinan, Shandong 250000, China

^f Department of Radiation Oncology, Shandong Cancer Hospital and Institute, Shandong First Medical University and Shandong Academy of Medical Sciences, Jinan, Shandong 250000, China

^g Department of Pharmacology, Faculty of Veterinary Medicine, Cairo University, 12211 Giza, Egypt

^h Department of Medical Pharmacology, Medical Faculty, Ataturk University, Erzurum 25070, Turkey

ⁱ Clinic of General Surgery, Molecular Oncology and Immunotherapy, Rostock University Medical Center, Rostock 18059, Germany

^j Department of Health Technology and Informatics, The Hong Kong Polytechnic University, Hong Kong SAR, 999077, China

^k Department of Oncology, The Seventh Affiliated Hospital Sun Yat-sen University, Shenzhen, Guangdong 518107, China

ARTICLE INFO

Keywords:

Bufalin
Pancreatic cancer
Cancer cell membrane camouflaging
NOD2
Multidrug resistance

ABSTRACT

Aims: Multidrug resistance in pancreatic cancer poses a significant challenge in clinical treatment. Bufalin (BA), a compound found in secretions from the glands of toads, may help overcome this problem. However, severe cardiotoxicity thus far has hindered its clinical application. Hence, the present study aimed to develop a cell membrane-camouflaged and BA-loaded polylactic-co-glycolic acid nanoparticle (CBAP) and assess its potential to counter chemoresistance in pancreatic cancer.

Methods: The toxicity of CBAP was evaluated by electrocardiogram, body weight, distress score, and nesting behavior of mice. In addition, the anticarcinoma activity and underlying mechanism were investigated both *in vitro* and *in vivo*.

Results: CBAP significantly mitigated BA-mediated acute cardiotoxicity and enhanced the sensitivity of pancreatic cancer to several clinical drugs, such as gemcitabine, 5-fluorouracil, and FOLFIRINOX. Mechanistically, CBAP directly bound to nucleotide-binding and oligomerization domain containing protein 2 (NOD2) and inhibited the expression of nuclear factor kappa-light-chain-enhancer of activated B cells. This inhibits the expression of ATP-binding cassette transporters, which are responsible for chemoresistance in cancer cells.

Conclusions: Our findings indicate that CBAP directly inhibits NOD2. Combining CBAP with standard-of-care chemotherapeutics represents a safe and efficient strategy for the treatment of pancreatic cancer.

1. Introduction

Although the prognosis of some cancers, such as lung and breast

cancer, has significantly improved, that of pancreatic cancer remains undesirable (Siegel et al., 2023). One of the main reasons is that most patients are resistant to first-line chemotherapeutic drugs, including

* Corresponding authors.

** Corresponding authors at: Department of General Surgery and Institute of Precision Diagnosis and Treatment of Digestive System Tumors, Carson International Cancer Center, Shenzhen University General Hospital, Shenzhen University, Shenzhen, Guangdong 518055, China.

E-mail addresses: weiguang.li@polyu.edu.hk (W. Li), fangsh9@mail.sysu.edu.cn (S. Fang), doctorgongpeng@szu.edu.cn (P. Gong), xianbin.zhang@szu.edu.cn (X. Zhang).

<https://doi.org/10.1016/j.drup.2023.101005>

Received 3 June 2023; Received in revised form 14 August 2023; Accepted 19 August 2023

Available online 21 August 2023

1368-7646/© 2023 The Author(s). Published by Elsevier Ltd. This is an open access article under the CC BY-NC-ND license (<http://creativecommons.org/licenses/by-nc-nd/4.0/>).

gemcitabine and 5-fluorouracil (Huang et al., 2022; Sethy and Kundu, 2021; Wu et al., 2022). Therefore, developing efficient strategies to enhance the chemosensitivity of pancreatic carcinoma cells is a well-accepted strategy for the development of next-generation therapeutics.

Because of its excellent capacity to reverse chemoresistance by regulating multimolecular pathways, bufalin (BA), the most popular extracted compound from the skin glands of *Bufo gargarizans* Canto or *Duttaphrynus melanostictus* Schneider, is being evaluated in various cancers (Asrorov et al., 2023; Cheng et al., 2019). However, several studies have demonstrated that BA is a cardiac glycoside similar to digoxin that triggers acute cardiotoxicity, making the clinical application of BA unacceptable (Bick et al., 2002).

In contrast to traditional therapeutic drugs that are taken up via passive diffusion by normal and cancer cells, nanodrugs can be designed to specifically target cancer cells and are able to extravasate and infiltrate actively into solid tumors (Ashrafizadeh et al., 2022; Lu et al., 2022; Pacheco et al., 2023). In addition, nanoparticles with a diameter of approximately 100 nm accumulate preferentially in tumors by enhanced permeation and retention effects (Koo et al., 2011). Thus, nanotechnology is a promising strategy to reduce organ toxicity and enhance the anticarcinoma effect of loaded drugs. However, these exogenous nanodrugs are easily recognized and cleared by mononuclear phagocytes (Liu et al., 2022; Lopes et al., 2023), which limits their effectiveness. To overcome this limitation, cell membrane camouflaged nanoparticles (CPNs) have been developed. Several studies have proven that camouflaging is an efficient strategy for delivering drugs (Dhas et al., 2022; Valcourt et al., 2018). Homologous cell membranes allow CPNs to escape clearance by mononuclear phagocytes and effectively accumulate at tumor sites. Therefore, CPNs may have the greatest potential to reduce the cardiotoxicity of BA and thus accelerate clinical applications. However, to the best of our knowledge, no studies have evaluated the safety and efficacy of cell membrane camouflaged and BA-loaded nanoparticles (CBAP) in treating pancreatic cancer.

Previous studies have suggested that BA can reverse chemoresistance by multiple mechanisms (Chen et al., 2021; Miao et al., 2023). For example, some studies have suggested that BA impairs nuclear factor kappa-light-chain-enhancer of activated B cells (NF- κ B), a master target of oligomerization domain containing protein 2 (NOD2), and prevents the expression of classic ATP-binding cassette (ABC) transporters, such as ABCB1 and ABCG2, which are major drug efflux pumps (Nomoto et al., 2022; Zhan et al., 2020; Zhang et al., 2023). However, the direct molecular target of BA remains unclear. Clarifying this issue will provide potential targets for overcoming drug resistance in pancreatic cancer.

The goal of the present study was to evaluate whether CBAP is a promising approach to reverse chemoresistance in pancreatic cancer. Additionally, guided by computer-aided drug discovery, this study identified a direct target of BA and clarified the mechanism that BA reverses the resistance of pancreatic cancer cells by regulating the NOD2/NF- κ B/ABC transporter signaling pathway.

2. Materials and methods

2.1. Cell culture and reagents

The human pancreatic cancer cell lines PANC-1, SW1990, MIA PaCa-2, and CFPAC-1 were purchased from the China Center for Type Culture Collection (CCTCC) and cultured in a CO₂ incubator (ESCO, Singapore) with 5% CO₂ and 95% air at 37 °C. The gemcitabine (GEM)-resistant cell lines GEM-MIAPaCa-2 and GEM-PANC-1 were developed as described previously (El Amrani et al., 2019). SUIT-2 cells were derived from metastatic liver tumors of human pancreatic carcinoma and obtained from the Japanese Collection of Research Bioresources Cell Bank (Iwamura et al., 1987). These cells were cultured in Dulbecco's modified Eagle's medium (DMEM), which was purchased from HyClone (Logan, USA, catalog no. SH30243.01), and supplemented with 10% fetal bovine

serum (FBS, AusGeneX, Gold Coast, Australia, catalog no. FBS500-S) plus 100 units/mL penicillin and 100 μ g/mL streptomycin (Gibco, New York, USA, catalog no. 15140-122). LTC is an immortalized rat pancreatic stellate cell line that has been described previously (Jaster et al., 2005; Sparmann et al., 2004; Zhang et al., 2018). Bufalin (BA, catalog no. S7821), gemcitabine (GEM, catalog no. S1149), 5-fluorouracil (5-FU, catalog no. S1209), oxaliplatin (OXA, catalog no. S1224), irinotecan hydrochloride (IR, catalog no. S5026) and calcium levofolinate (catalog no. S2588) were obtained from Selleck Chemicals (Houston, USA). GSK717 (catalog no. HY-136555), the traditional inhibitor of NOD2, PPQ-102 (catalog no. HY-14179), the inhibitor of cystic fibrosis transmembrane conductance regulator (CFTR), and bafilomycin A1 (BAFA1, catalog no. HY-100558) were obtained from MedChemExpress (Monmouth Junction, USA). Chloroquine diphosphate salt (CQ) was obtained from Sigma-Aldrich (St. Louis, USA, catalog no. C6628).

2.2. Evaluating the antitumor activity of therapeutics in vitro

To evaluate cell viability, pancreatic cancer cells or LTC cells were seeded at 4×10^3 cells per well onto a 96-well plate. On the following day, these cells were treated with GEM, BA, PNs, CPNs, or CBAP at the indicated concentrations. After 24 h, cell viability was evaluated by the cell counting kit-8 (CCK-8, MedChemExpress, catalog no. HY-K0301), and the absorbance was determined at 450 nm using a Synergy LX multimode reader (BioTek, Winooski, USA). For assessment of cell death, pancreatic cancer cells were seeded at 7×10^5 per well in a 6-well plate and allowed to grow for 24 h. Subsequently, these cells were treated with vehicles, 0.5 μ M BA, 10 μ M GEM, or 0.5 μ M BA plus 10 μ M GEM for 24 h. The calcein-AM/PI double stain kit (Yeasen, Shanghai, China, catalog no. 40747ES76) was used to stain the cells (Du et al., 2022). In addition, to verify the results of calcein-AM/PI double staining, trypan blue assays were performed to determine the percentage of dead cells (Zhang et al., 2019b). Cells were treated with 0.05 μ M CBAP, 10 μ M GEM, 100 μ M 5-FU, 1 μ M OXA, FOLFORINOX (the dosage is 0.01-fold of that used in the clinic, containing 116 μ M OXA, 167 μ M IR, 361 μ M folinic acid, and 1.67 mM 5-FU) or the corresponding drug combination. After 24 h, in order to evaluate the percentage of dead cells, trypan blue assay was performed and the data was calculated as follows: Percentage of cell death (%) = $100\% \times \text{dead cells} / (\text{dead cells} + \text{alive cells})$. The Q value was calculated according to the method reported by Jin (1980). Q value > 1.15 indicates that the combinational therapy has a synergistic effect; $0.85 < \text{Q value} < 1.15$ represents a simple additive effect, and Q value < 0.85 indicates an antagonistic effect. To evaluate apoptosis and necrosis, MIA PaCa-2 cells were seeded at 7×10^5 cells per well in a 6-well plate and treated with vehicles, 10 μ M GEM, 0.5 μ M CBAP, 100 μ M GSK717, 10 μ M PPQ-102 or the indicated drug combination for 24 h. The percentage of apoptotic cells was determined with the help of Annexin V-APC/PI apoptosis kit (Elabscience, Houston, USA, catalog no. E-CK-A217) and a NovoCyte flow cytometer system (Agilent, Santa Clara, USA) using the following formula: $100\% \times (\text{Annexin V-APC}^+\text{PI}^- + \text{Annexin V-APC}^+\text{PI}^+) \text{ cells} / \text{total cells}$. The percentage of necrotic cells was calculated by the formula $100\% \times \text{Annexin V-APC}^+\text{PI}^+ \text{ cells} / \text{total cells}$ (Chen et al., 2008; Jiang et al., 2016).

2.3. Testing organ toxicity of BA

We intraperitoneally injected mice with 10 mg/kg, 2 mg/kg, or 1 mg/kg BA, and the mortality rate of the mice was determined. In previous studies, we developed and investigated the performance of some noninvasive methods, such as animal distress score, body weight and nesting activity, in evaluating the side effects and organ toxicity of drugs (Zhang et al., 2020a). In the present study, to evaluate the toxicity of BA, the distress score was determined at -30 min (min), 0 min, 30 min, 60 min, 120 min, and 240 min after injection of 1 mg/kg BA (N = 6). To evaluate the nesting activity of mice, they were placed in individual

cages one hour before the dark phase, as reported by previous studies (Deacon, 2012; Kumstel et al., 2020a). After injection of chemical drugs, a 1.0 g cotton ball was immediately provided, and the nesting score was determined in the next morning.

For assessment of cardiotoxicity, the electrocardiography (ECG) signal of mice was recorded by a biological signal acquisition system (Yuyan Instruments, Shanghai, China). To evaluate drug toxicity to the heart, liver and kidney, blood samples were taken from mice, and cardiac troponin I, aspartate aminotransferase (AST), alanine transaminase (ALT), creatinine (CREA), urea, and uric acid (UA), were determined.

2.4. Synthesis of the cell membrane-camouflaged bufalin delivery system

To develop the bufalin-loaded PNs (BAP), 100 μ L of 5 mg/mL BA, 200 μ L of 10 mg/mL polylactic-co-glycolic acid (PLGA), 200 μ L of 16 mg/mL D- α -tocopheryl polyethylene glycol succinate (TPGS), and 300 μ L acetone were premixed and dropped slowly into 4 mL deionized water under stirring. Cell membrane vesicles (CMVs) were harvested and extracted from MIA PaCa-2 cells as described previously (Zhang et al., 2019a). These membranes were mixed with BAP, extruded through a 200 nm porous membrane with the help of an extruder (Avanti, Hilleroed, Denmark) and subsequently sonicated in an ice bath. To optimize the CBAP process, different weight ratios of PLGA to BA, such as 20:1, 10:1, 5:1 and 2:1 (the corresponding molar ratios are 1:2.3, 1:4.7, 1:9.3 and 1:23.3), were evaluated. Subsequently, the drug loading capacity and encapsulation efficiency were determined as described previously (Zhang et al., 2021).

2.5. Characterization of the cell membrane-camouflaged bufalin delivery system

The morphology of the nanoparticles was characterized by an HT7800 transmission electron microscope (TEM, Hitachi, Tokyo, Japan). The size distribution, zeta potential, and stability in PBS (pH = 7.4) containing 10% FBS, PBS (pH = 7.4) and PBS (pH = 5.0) were determined by Zetatronix 919 (Opptronix, Shanghai, China). To verify if we successfully developed the cell membrane-camouflaged bufalin delivery system, samples including PNs, CPNs, CMVs and cancer cells were lysed and boiled. Subsequently, total proteins were visualized with the support of sodium dodecyl sulfate-polyacrylamide gel electrophoresis (SDS-PAGE), and indicators of the cell membrane, mitochondria or cytoplasm were determined with the support of Western blot and the following antibodies (Chen et al., 2016; Yan et al., 2022): anti-Galectin 3 (ABclonal, Wuhan, China, catalog no. A11198, dilution: 1000 \times), anti-EPCAM (Beyotime, Shanghai, China, catalog no. AF0141, dilution: 1000 \times), anti-COX IV (Cell Signaling, Danvers, USA, catalog no. 4850, dilution: 1000 \times) and anti- β -Actin-peroxidase (Sigma-Aldrich, catalog no. A3854, dilution: 40000 \times). Proteins were visualized using an ultrasensitive enhanced chemiluminescence kit (New Cell and Molecular Biotech, Suzhou, China, catalog no. P10300) and MiniChemTM 610 chemiluminescent imaging system (Sage Creation Science, Beijing, China). In addition, the CPNs were evaluated by colocalization analysis as described in our previous study (Zhang et al., 2021) with the support of an Axio Vert. A1 fluorescence microscope (Carl Zeiss, Oberkochen, Germany).

2.6. Evaluating cellular uptake of the cell membrane-camouflaged bufalin delivery system

To determine CPNs by fluorescence microscopy, the PNs and CMVs were labeled with 3,3'-diiodoacetyl carbocyanine perchlorate (DiO, Meilunbio, Dalian, China, code MB4239) and 1,1'-diiodoacetyl-3,3',3'-tetramethylindocarbocyanine perchlorate (DiI, Meilunbio, code MB4240), respectively. To evaluate the cellular uptake ability of nanoparticles, 7×10^5 MIA PaCa-2 cells per well were allowed to grow in a 6-well plate for 24 h and incubated with DiI- and DiO-labeled CPNs for 3 h.

The cell nucleus was stained using 4',6-diamidino-2-phenylindole (DAPI, Beyotime, catalog no. C1002). To evaluate the cellular uptake of CPNs, cells were incubated with DiI-labeled CPNs for different time periods or with different ratios of CMVs and PNs. Subsequently, the cellular uptake of nanoparticles was evaluated by a NovoCyte flow cytometer system.

2.7. Orthotopic xenograft model and subcutaneous xenograft model

The animal experiments were approved by the Institutional Animal Care and Use Committee of Shenzhen University and Peking University. Six-week-old male BALB/c nude mice were purchased from Vital River (Beijing, China) and fed standard laboratory chow and water ad libitum. To evaluate the anticarcinoma activity of the therapeutics, the mice were anesthetized with 1.2–2.5% isoflurane. A transverse incision was made below the liver. The duodenum and pancreas were fixed by a cotton swab, and 5 μ L of 1×10^6 cells/ μ L MIA PaCa-2 suspension was injected into the pancreatic head using a precooled Hamilton syringe (Reno, USA). After placing the pancreas in the abdominal cavity, the cavity was closed with a coated 5–0 Vicryl suture. On the fourth day after cell injection, mice were weighed and randomly divided into six groups. Subsequently, they were intravenously treated with vehicles (N = 15), 1 mg/kg CBAP (N = 15), 50 mg/kg GEM (N = 15), or 25 mg/kg 5-FU (N = 15) twice a week. For combinatorial treatment (N = 15), mice were intravenously injected with 1 mg/kg CBAP, and after 24 h, they were treated with 50 mg/kg GEM or 25 mg/kg 5-FU via the tail vein. On the 40th day after cell injection, mice were sacrificed, and the tumor weight was determined. To observe the distribution of nanoparticles, a subcutaneous xenograft model was developed. Briefly, 100 μ L of 1×10^7 MIA PaCa-2 cells was subcutaneously inoculated into the right flank of nude mice, and IR783 (Aladdin, Shanghai, China, catalog no. I157644)-labeled PNs or CPNs were intravenously injected. The distribution of the nanoparticles was observed at predetermined time intervals by an Ani-View600 multimode animal *in vivo* imaging system (Biolight Biotechnology, Guangzhou, China).

2.8. Western blot

To perform the Western blot assay, 4×10^5 pancreatic cancer cells or GEM-resistant cancer cells per well were grown in 6-well plates for 24 h and followed by the incubation of 0.05 μ M BA, 0.05 μ M CBAP, 50 μ M GSK717, 5 μ M CQ, 0.2 μ M bafilomycin A1 (BAFA1) or 10 μ M PPQ-102 in the presence or absence of GEM for 6, 12 or 24 h, and the Western blot was performed as previously described (Zhang et al., 2020b) using the following antibodies: anti-NOD2 (ABclonal, catalog no. A15992, dilution: 1000 \times), anti-ABCB1 (Proteintech, Chicago, USA, catalog no. 22336-1-AP, dilution: 1000 \times), anti-ABCG2 (Proteintech, catalog no. 27286-1-AP, dilution: 1000 \times), anti-CFTR (ABclonal, catalog no. A8386, dilution: 1000 \times), β -Actin-peroxidase antibody (Sigma-Aldrich, catalog no. A3854, dilution: 40000 \times), anti-Pdx1 (Cell Signaling, catalog no. 5679, dilution: 1000 \times), anti-PSPC-1 (Proteintech, catalog no. 16714-1-AP, dilution: 1000 \times), anti-NF- κ B p65/RelA (ABclonal, catalog no. A19653, dilution: 1000 \times), recombinant anti-Lamin A+C antibody (Abcam, Cambridge, UK, catalog no. ab133256, dilution: 1000 \times), anti-LC3B (ABclonal, catalog no. A19665, dilution: 1000 \times), anti-SQSTM1/p62 (ABclonal, catalog no. A19700, dilution: 1000 \times), anti-DFNA5/GSDME (Abcam, catalog no. ab215191, dilution: 1000 \times).

2.9. Tandem RFP-GFP-targeted LC3 fluorescence microscopy and transmission electron microscopy

To evaluate autophagic flux, 2×10^5 MIA PaCa-2 cells per well were seeded one day prior to infection in a 12-well plate on 20-mm round glass coverslips. On the following day, the cells were transfected with RFP-GFP-targeted LC3 plasmid (Addgene, Watertown, USA, catalog no. 21074) using Lipofectamine 3000 (Thermo Fisher Scientific, Waltham,

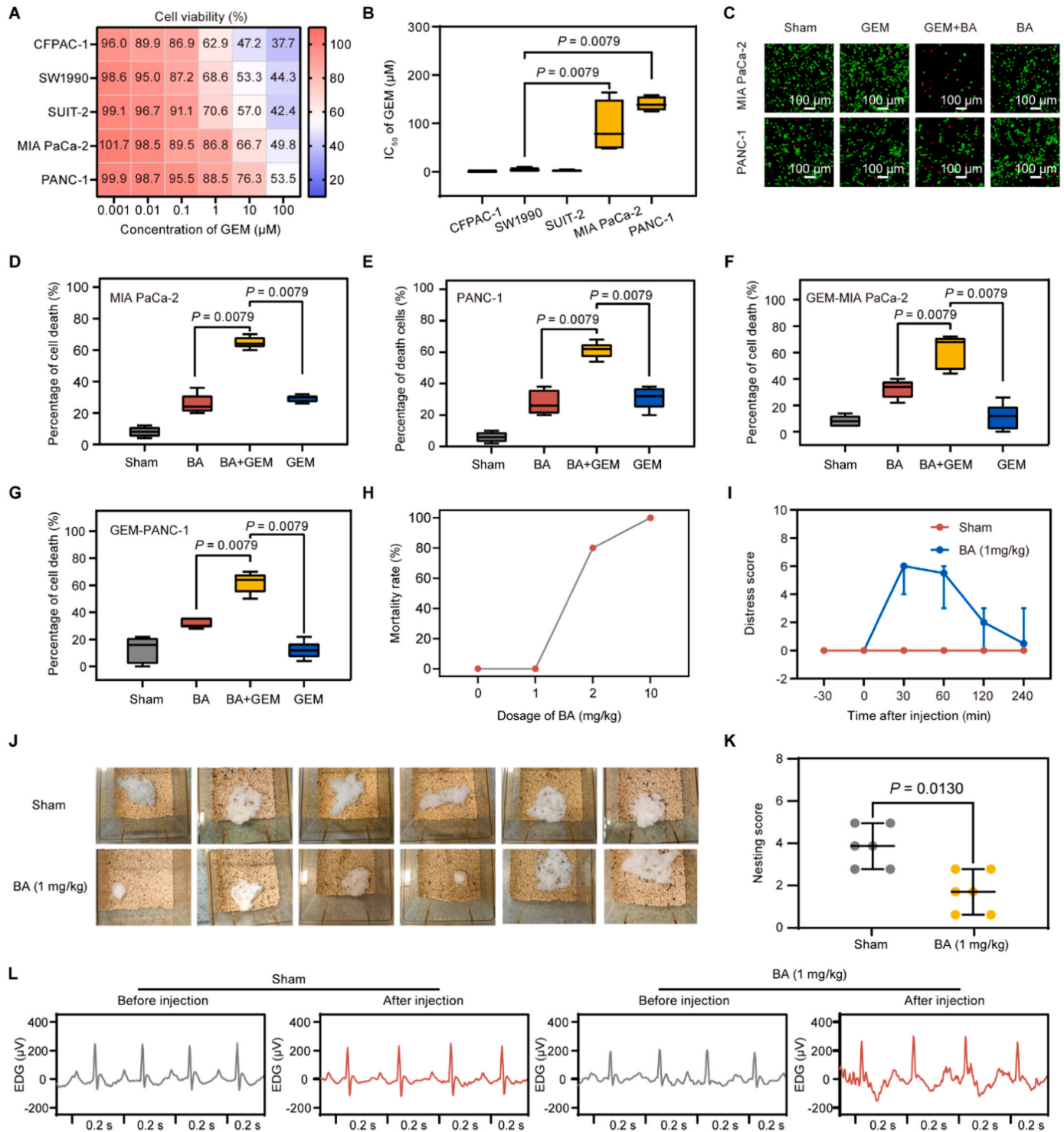


Fig. 1. Evaluating the antitumor effect and organ toxicity of BA. After treating cells with different dosages of GEM, the cell viability (A) and IC₅₀ (B) of GEM were determined. These data suggested that both MIA PaCa-2 and PANC-1 are intrinsically resistant to GEM. The calcein-AM/PI assay (C) and trypan blue staining proved that BA synergistically increased GEM-mediated cell death in MIA PaCa-2 (D) and PANC-1 (E) cells. Additionally, BA was observed to increase chemosensitivity in the acquired GEM-resistant cell lines GEM-MIA PaCa-2 (F) and GEM-PANC-1 (G). However, BA had severe organ toxicity, which was determined by the mortality rate (H), distress score (I), nesting behavior (J and K) and ECG (L). N = 5 for (A-B); N = 5 for (D-G); N = 6 for (I-K).

USA, catalog no. L3000001), and the autophagic flux was determined with the support of an ECLIPSE Ti2 confocal microscope (Nikon, Tokyo, Japan) after treating cells with 0.05 µM CBAP for 24 h. In order to evaluate the autophagy and pyroptosis by TEM, 7 × 10⁵ MIA PaCa-2 cells per well were seeded into 6-well plates for 24 h. These cells were treated with 0.05 µM CBAP, 10 µM GEM, or the drug combination for

another 24 h and fixed using 2.5% glutaraldehyde in 0.1 M cacodylate buffer. After preembedding, dehydration and polymerization were performed. The cell samples were ultrathin sectioned by a Leica EM UC7 ultramicrotome (Leica, Wetzlar, Germany) and stained with 2% uranium acetate saturated alcohol solution. The images were obtained with the support of a HT7800 TEM.

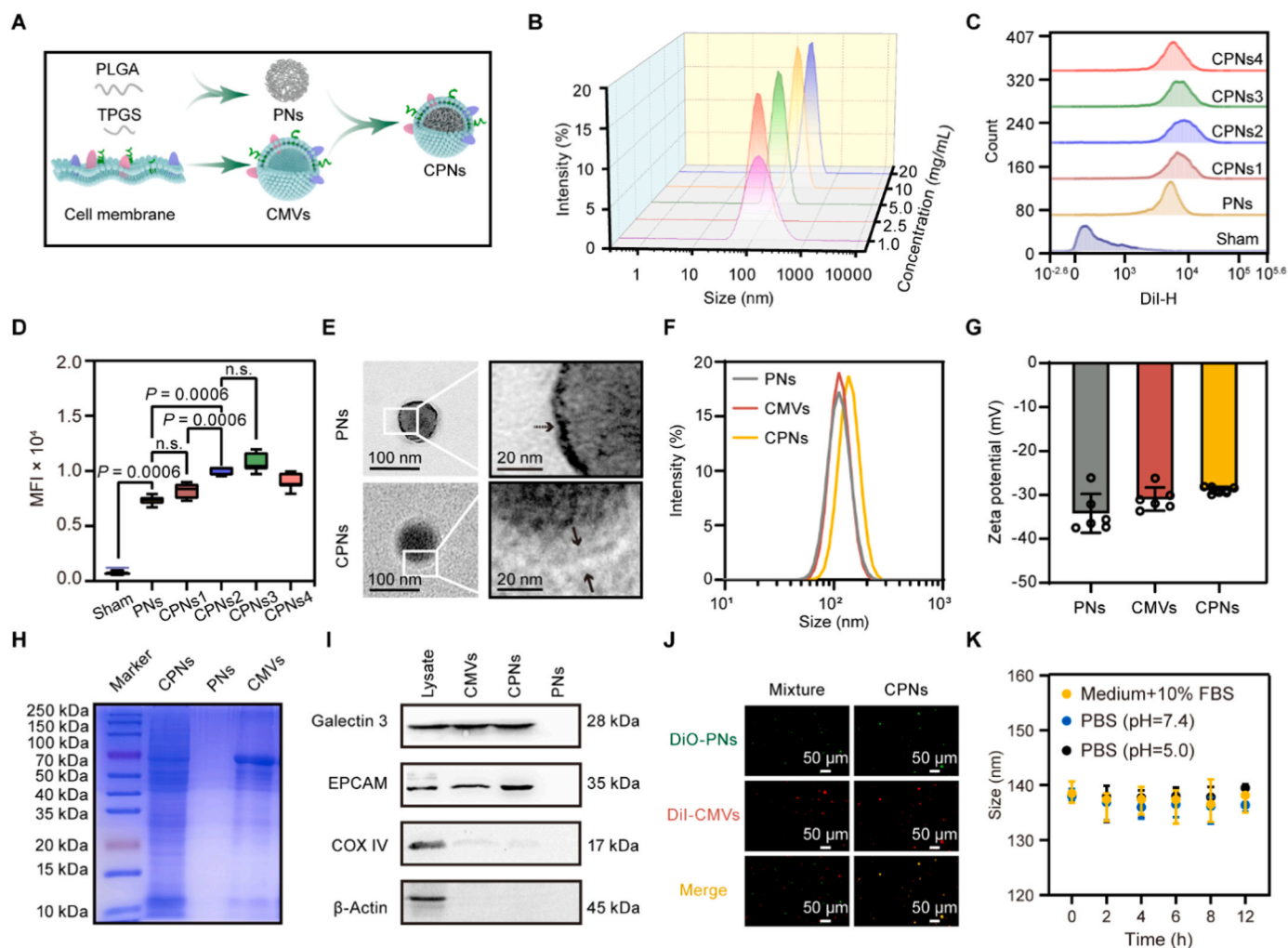


Fig. 2. Development and characterization of CPNs. The cell membrane-camouflaged delivery system for BA was developed using PLGA, TPGS, and cancer cell membrane (A). To obtain the optimized size of CPNs, different concentrations of PLGA were evaluated (B). The optimal ratio of PNs to CMVs was 1:0.5, at which CPNs could be significantly endocytosed by the tumor cells (C and D). TEM (E), size distribution (F) and zeta potential (G) were used to characterize the morphology of PNs, CMVs (positive control), and CPNs. SDS—PAGE (H), Western blot (I), and fluorescence colocalization (J) were applied to verify that the membrane was successfully coated the surface of PNs. In addition, the size of CPNs in different media remains constant (K). N = 7 for (C-D); N = 6 for (G).

2.10. RNA sequencing

To evaluate if and how CBAP regulates the expression of ABC transporters, 4×10^5 MIA PaCa-2 cells per well were grown in 6-well plates for 24 h. These cells were treated with 0.5 μ M CBAP for 24 h. RNA was extracted using TRIzol (Thermo Fisher Scientific, catalog no. 15596026), and Illumina next-generation sequencing was used to evaluate the expression of mRNA. The DESeq2 package in R was applied to determine the differentially expressed genes with $p_{\text{adj}} < 0.05$ and $|\log_2(\text{fold change})| > 1$.

2.11. Molecular docking

To compare the communication between inhibitors and the target protein NOD2, a virtual molecular docking approach was used in the present study. The structure of human NOD2 protein was predicted by AlphaFold (<https://alphafold.ebi.ac.uk/entry/Q9HC29>), and the 3D structures of BA (Compound CID: 9547215) and GSK717 (Compound CID: 102369397) were obtained from PubChem. The docking pocket of NOD2 was predicted by the DoGSiteScorer method in ProteinsPlus. Subsequently, molecular docking was performed using AutoDock Vina, in which docking pockets constructed by AutoDockTools were centered at -1.76 \AA , 2.57 \AA , and -1.96 \AA with sizes of $23.25 \text{ \AA} \times 27.0 \text{ \AA} \times 47.25$

 \AA . Subsequent molecular interaction and visualization were achieved by PyMOL.

2.12. Statistical analysis

The results are presented as medians with 95% confidence intervals. The Mann-Whitney rank sum test followed by Bonferroni correction was applied to evaluate the significant differences, and a P value lower than 0.05 divided by the number of meaningful comparisons was considered significant.

3. Results

3.1. BA reverses the resistance of pancreatic cancer to GEM

To determine intrinsic drug resistance, the cell lines CFPAC-1, SW1990, SUIT-2, MIA PaCa-2, and PANC-1 were treated with GEM (Fig. 1A). Compared to other cell lines, MIA PaCa-2 and PANC-1 cells exhibited the highest resistance to GEM (Fig. 1B). Subsequently, the effect of BA on intrinsic chemoresistance was evaluated in these two cell lines. We observed that the combinational therapy increased the percentage of dead cells compared to cells treated with 10 μ M GEM (Fig. 1C). This is supported by trypan blue assay, which proved that 0.5

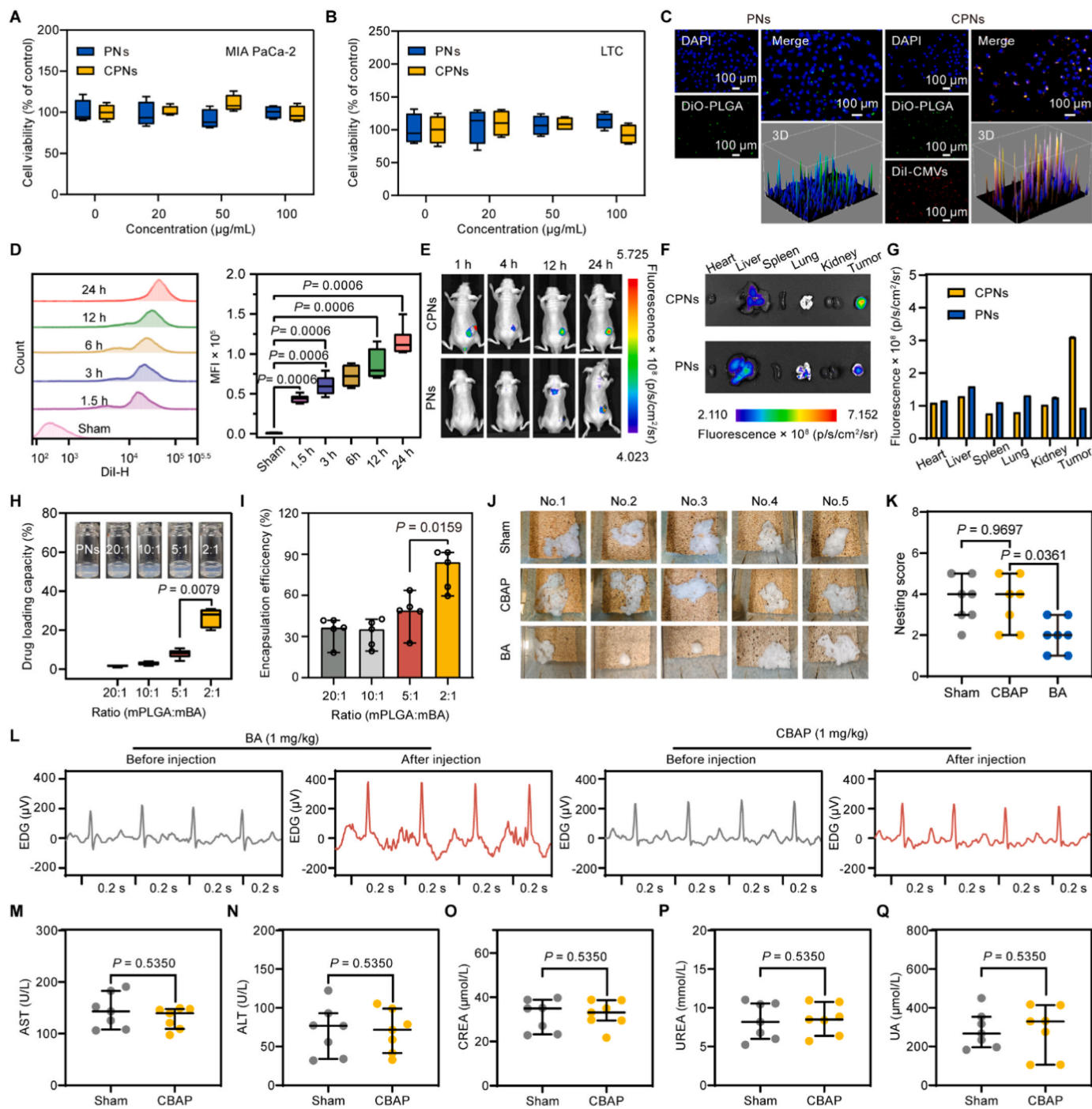


Fig. 3. Investigating the efficacy and safety of CPNs for the delivery of BA. CCK-8 analysis proved that the delivery system, CPNs, had no effect on the growth of tumor cells (A) and cells in the tumor environment (B). Fluorescence microscopy showed that compared to PNs (green dots), more CPNs (yellow dots) were absorbed by tumor cells (C). Indeed, the cellular uptake of CPNs was increased in a time-dependent manner (D). *In vivo* fluorescent images (E) and *ex vivo* results (F and G) also proved that CPNs are superior to PNs in the delivery of BA to the tumor sites. When the mass ratio of PLGA to BA was 2:1, CBAP had great drug loading capacity (H) and encapsulation efficiency (I). The nesting score (J and K) and ECG (L) proved that CBAP eliminated the cardiotoxicity of BA. Moreover, the biochemical blood test demonstrated that CBAP did not impair the functions of the liver (M and N) or kidney (O-Q). N = 4 for (A-B); N = 7 for (D); N = 7 for (M-Q).

μM BA synergistically increased GEM-induced cell death in intrinsic GEM-resistant pancreatic cancer cells, MIA PaCa-2 (Fig. 1D) and PANC-1 (Fig. 1E). Next, we established two acquired GEM-resistant cell lines, GEM-MIA PaCa-2 and GEM-PANC-1, and we observed that IC_{50} of these two cell lines were significantly higher than those corresponding parental cell lines (Fig. S1). We then evaluated the effect of BA in GEM-MIA PaCa-2 (Fig. 1F) and GEM-PANC-1 (Fig. 1G). We found that $0.5 \mu\text{M}$ BA significantly decreased the resistance of cells to GEM. These results,

in summary, suggest that BA can significantly increase the sensitivity of pancreatic cancer cells to GEM.

To evaluate the benefit of BA *in vivo*, we performed a preliminary experiment and intraperitoneally injected 10 mg/kg, 2 mg/kg, or 1 mg/kg BA into mice. We observed that the animals developed cardiac glycoside poisoning symptoms, such as palpitations, shortness of breath, and convulsions. As indicated in Fig. 1H, only a few mice survived after treated with 10 mg/kg BA or 2 mg/kg BA. Although 1 mg/kg BA did not

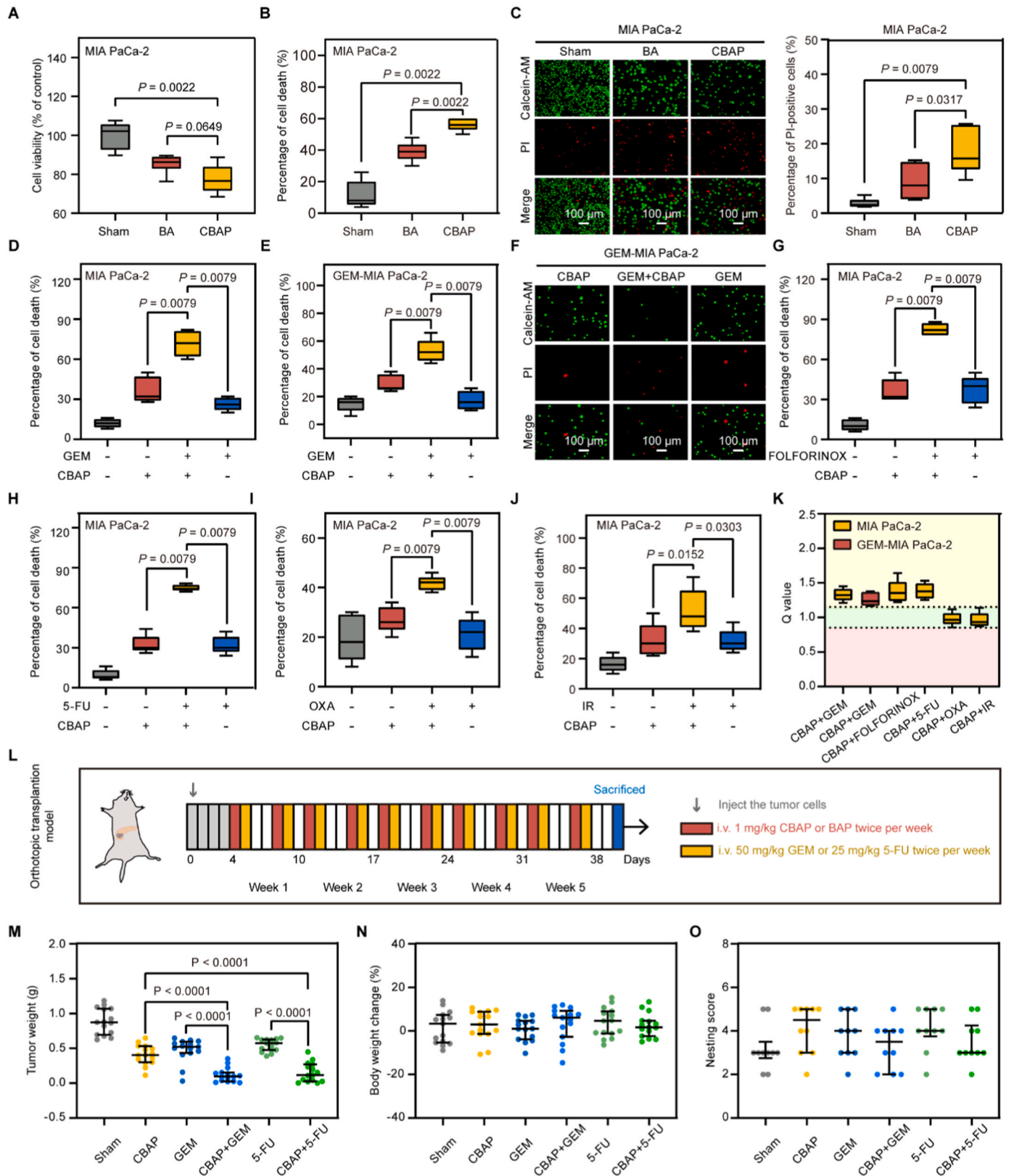


Fig. 4. Evaluating the benefit and safety of CBAP and its combination with distinct chemotherapeutic agents *in vitro* and *in vivo*. CCK-8 (A), trypan blue (B), and calcein-AM/PI (C) analyses suggested that the anticarcinoma activity of CBAP was superior to that of BA. In addition, CBAP enhanced sensitivity to GEM in both MIA PaCa-2 (D) and GEM-MIA PaCa-2 cell lines (E and F). Moreover, although CBAP significantly increased chemotherapeutic agents-induced cell death (G-J), the Q value indicated that only the combinational strategies of CBAP plus GEM, CBAP plus FOLFORINOX and CBAP plus 5-FU synergistically induced cell death (K). The orthotopic xenograft model (L) also proved that CBAP significantly enhanced the antitumor effect of GEM and 5-FU (M). In addition, CBAP did not affect the body weight (N) or nesting score (O). N = 6 for (A-B); N = 5 for (C-E); N = 5 for (G-I); N = 6 for (J); N = 15 for (M-O).

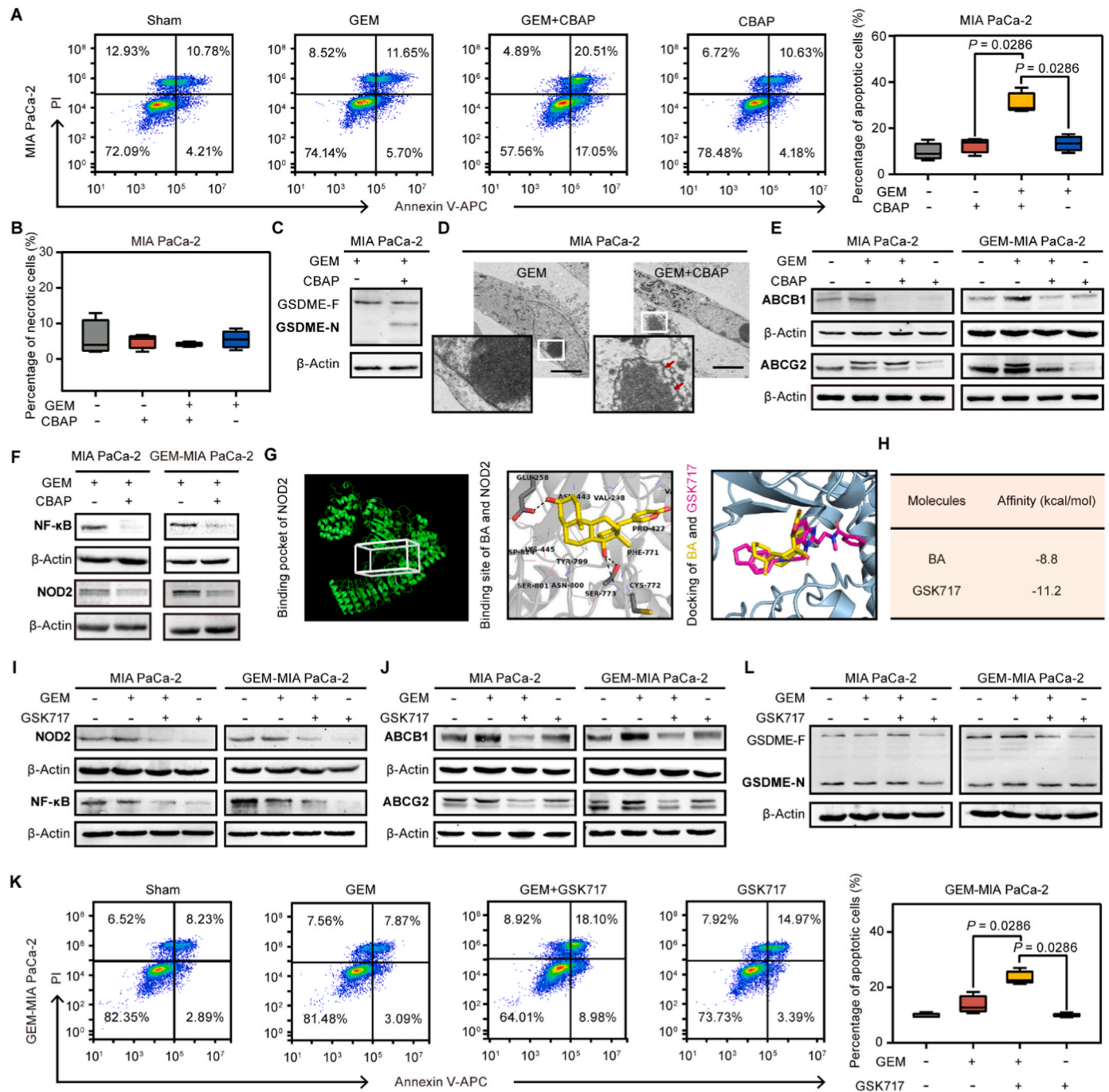


Fig. 5. Clarifying the molecular mechanism by which CBAP reverses GEM resistance by reducing the expression of classic ABC transporters. Flow cytometry proved that compared to GEM monotherapy, CBAP plus GEM significantly increased apoptosis (A) but did not influence necrosis (B) in pancreatic cancer cells. Western blot and TEM suggested that the combinational therapy induced pyroptosis (C and D). Mechanistically, we observed that CBAP inhibited the expression of ABCB1 and ABCG2 (E) and decreased the expression of NF- κ B and NOD2 (F). In addition, AlphaFold and molecular docking (G and H) implied that similar to GSK717, BA directly binds to NOD2, the classic regulator of NF- κ B. Indeed, inhibition of NOD2 activity could impair the expression of NF- κ B (I) and ABC transporters (J). This increased GEM-induced apoptosis (K), but did not influence pyroptosis (L). N = 4 for (A-B); N = 4 for (K).

impair the survival of mice, it significantly increased the distress score (Fig. 1I) and decreased the nesting score (Fig. 1J and K), which we developed and proved to be a sensitive strategy in evaluating the toxicity of drugs (Kumstel et al., 2020a; Kumstel et al., 2020b). In addition, inverted T waves were observed in the electrocardiogram (ECG) after injection of 1 mg/kg BA (Fig. 1L). This indicated that BA caused severe acute cardiotoxicity.

3.2. Development and characterization of CPNs

To decrease the accumulation of BA in the heart and reduce its cardiotoxicity, PLGA nanoparticles (PNs) were developed and camouflaged by cell membrane vesicles (CMVs) (Fig. 2A). As indicated in Fig. 2B, to optimize the development process of CPNs, various concentrations of PLGA were investigated. We observed that when the concentration of PLGA is 2.5 mg/mL, the size of synthesized nanoparticles is around 100 nm. This is an optimal size for nanoparticles according to the

literatures (Duan and Li, 2013; Li et al., 2023; Wang et al., 2015). Consequently, this concentration was selected for the subsequent experiments. To determine the optimal ratio of PNs to CMVs, carcinoma cells were incubated with vehicles (Sham), PNs, CPNs1 (1:0.25), CPNs2 (1:0.5), CPNs3 (1:1) and CPNs4 (1:2), and the mean fluorescence intensity (MFI) was determined. We observed that CPNs2 significantly increased the MFI of carcinoma cells compared to vehicles (Sham), PNs, and CPNs1 (Fig. 2C and D). In addition, we observed that CPNs were covered by membranes (Fig. 2E). Moreover, the size distribution (Fig. 2F) and zeta potential (Fig. 2G) were similar to those of CMVs. Therefore, we used this ratio (PN: CMV at 1:0.5) for subsequent experiments. To verify the CPNs, the membrane proteins and cytoplasmic proteins were determined by SDS-PAGE and Western blot. This indicated that CPNs and CMVs loaded proteins compared to PNs (Fig. 2H), and these proteins are membrane proteins, such as Galectin 3 and EPCAM (Fig. 2I). We did not observe COX IV (mitochondrial protein) and β -Actin (cytoplasmic protein) in CMVs and CPNs (Fig. 2I), which suggested that the cytoplasmic and mitochondrial proteins were successfully removed. In addition, a fluorescent colocalization assay was conducted to observe the membrane coating on PNs (Fig. 2J). In the mixture group, red and green dots were randomly distributed. However, the green fluorescent signal of DiO-PNs and the red fluorescence of DiI-CMV were superimposed together in CPNs, resulting in yellow dots (Fig. 2J). We determined the size of nanoparticles at 2–12 h and observed that the size did not change over time. This suggests that CPNs is stable (Fig. 2K).

3.3. CBAP is a safe and efficient treatment for pancreatic cancer

To investigate whether CPNs influence the viability of pancreatic cancer cells (Fig. 3A) and the cells in the tumor environment (Fig. 3B), we incubated the cells with different concentrations of PNs and CPNs and observed that neither PNs nor CPNs significantly affected the viability of carcinoma cells (Fig. 3A) or LTC cells (Fig. 3B). This suggests that CPN is a safe strategy for the delivery of BA. To observe the cellular uptake of PNs and CPNs, PLGA and CMVs were labeled with DiO and DiI, respectively. Compared to PNs, a large amount of CPNs were observed inside cells. Meanwhile, we can observe that the red fluorescence is overlapped with green fluorescence in CPNs (Fig. 3C). In addition, we observed a time-dependent increase of MFI in MIA PaCa-2 cells (Fig. 3D). To evaluate the cellular uptake of CPNs *in vivo*, IR783-labeled PNs or CPNs were injected into the tail vein of mice, and the fluorescence was determined. When compared to PNs, the accumulation of CPNs at tumor site was high (Fig. 3E). In addition, *ex vivo* fluorescent images proved that CPNs preferentially accumulated in the tumor when it was compared to other organs, such as the heart, liver, spleen, lung, and kidney (Fig. 3F and G).

To evaluate the efficacy of CPNs, the drug loading capacity (Fig. 3H) and encapsulation efficiency (Fig. 3I) were investigated. When the mass ratio of PLGA to BA was 2:1, the delivery system had acceptable encapsulation efficiency (Fig. 3I). Therefore, we used this ratio to develop the CBAP. To evaluate the toxicity of CBAP, we investigated the nesting score and cardiotoxicity. We observed that compared to Sham,

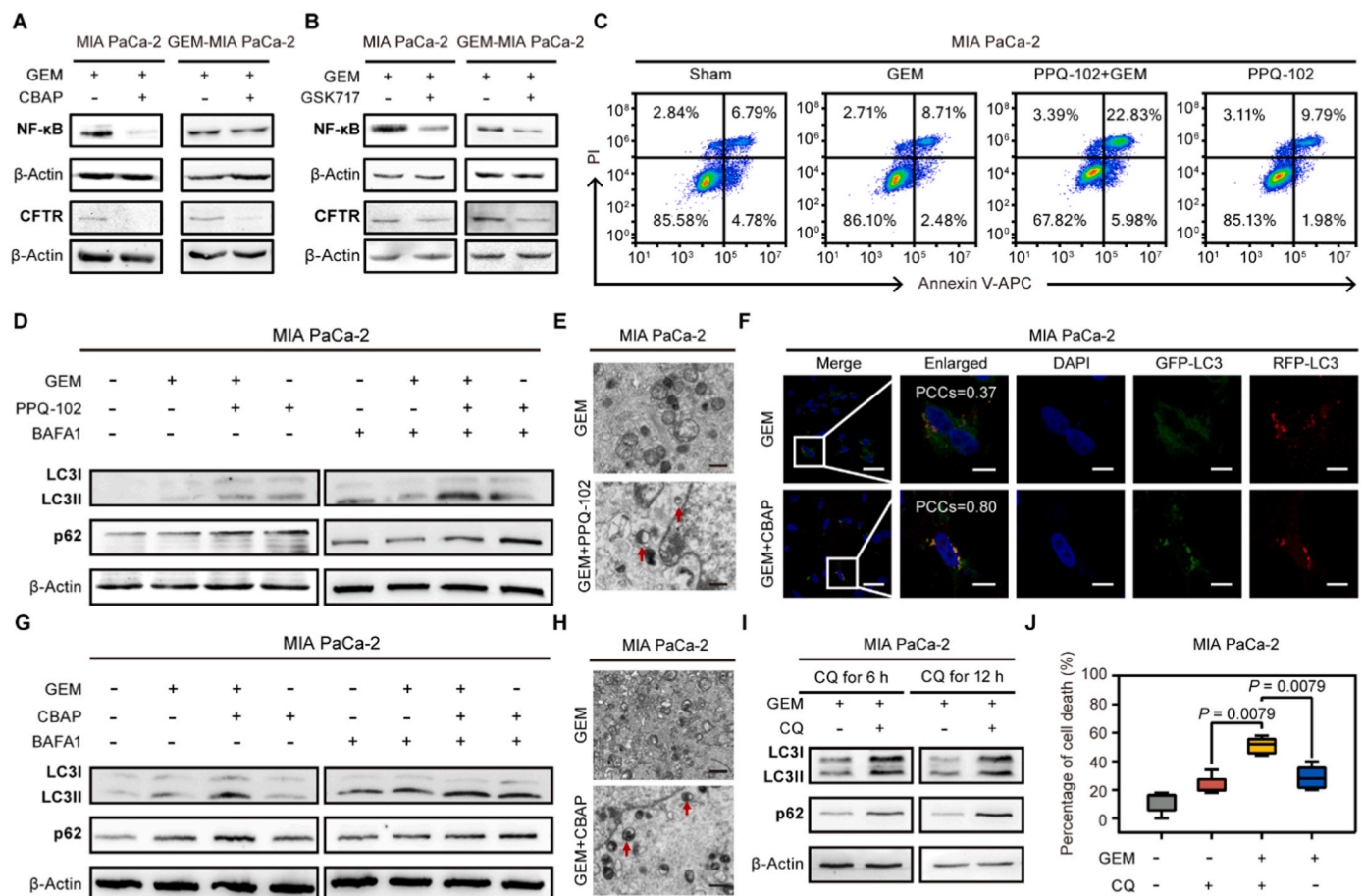


Fig. 6. Elucidation of the molecular mechanism by which CBAP overcomes chemoresistance by reducing CFTR, an unclassified ABC transporter. Western blot assays suggested that both CBAP (A) and GSK717 (B) inhibited the expression of CFTR and NF- κ B in cancer cells. Inhibition of CFTR by PPQ-102 increased the anticarcinoma activity of GEM by influencing apoptosis (C). In addition, we observed that inhibition of CFTR blocked autophagic flux via Western blot (D), TEM (E) and confocal microscopy (F), which is similar to the effect of CBAP (G and H). We found that blocking autophagy by CQ could increase GEM-induced cell death (I and J). N = 4 for (C); N = 5 for (J).

CBAP did not influence the nesting score (Fig. 3J and K), and most importantly, it did not induce cardiotoxicity (Fig. 3L). Additionally, blood biochemical results suggested that CBAP did not impair the functions of the heart (Fig. S2), liver (Fig. 3M and N) and kidney (Fig. 3O-Q).

3.4. CBAP reversed multiple drug resistance in pancreatic cancer

To evaluate the benefit of CBAP in treating pancreatic cancer, cell viability (Fig. 4A) and cell death (Fig. 4B) were determined. The anticarcinoma activity of 0.5 μM CBAP was slightly superior to that of 0.5 μM BA (Fig. 4A and B). Very similar results were obtained by the calcein-AM/PI double staining assay. Compared to BA-treated cells, the percentage of PI-positive cells increased in CBAP-treated cells (Fig. 4C).

To evaluate the benefit of CBAP in the reversal of multiple drug resistance, 0.5 μM CBAP in combination with 10 μM GEM was used to treat MIA PaCa-2 cells (Fig. 4D). We observed that 0.5 μM CBAP and 10 μM GEM slightly induced cell death; however, the combinational therapy significantly induced cell death when compared to each monotherapy (Fig. 4D). The benefit of CBAP in distinct chemotherapeutic strategies was also evaluated in GEM-resistant pancreatic cancer cells (Fig. 4E and F) and parental cells (Fig. 4G-J). The Q value indicated that CBAP not only increased the sensitivity of pancreatic cancer cells to GEM but also synergistically increased the anticarcinoma activity of 5-FU (Fig. 4K). However, it did not reverse the resistance to OXA or IR (Fig. 4K). To confirm the *in vitro* results, the combinational therapies CBAP plus GEM and CBAP plus 5-FU were evaluated in an orthotopic xenograft model (Fig. 4L). Compared to monotherapy, the combinational therapies significantly decreased the tumor weight (Fig. 4M), but they did not significantly change the body weight (Fig. 4N) or nesting score (Fig. 4O). These findings support that CBAP could be a safe and efficient strategy for the treatment of pancreatic cancer.

3.5. CBAP enhanced chemosensitivity by directly targeting NOD2

To clarify how CBAP enhanced the chemosensitivity of pancreatic cancer cells to chemical drugs, we first determined the forms of cell death after incubation of the cells with CBAP and GEM. CBAP significantly increased GEM-induced apoptosis (Fig. 5A); however, it did not influence necrosis (Fig. 5B). Furthermore, CBAP elevated the levels of N-terminal fragment of GSDME (GSDME-N), which punched holes in the cell membrane and resulted in pyroptosis (Fig. 5C and D).

To evaluate whether ABC transporters were involved in CBAP-mediated chemosensitivity, we evaluated the expression of ABCB1 and ABCG2, two classic transporters known to be involved in GEM resistance (Fig. 5E). To investigate how CBAP regulates the expression of these transporters, we determined the expression of paraspeckle component 1 (PSPC1), pancreatic duodenal homeobox gene-1 (Pdx1) and nuclear factor kappa-light-chain-enhancer of activated B cells (NF- κ B) (Fig. S3). We observed that CBAP decreased the expression in cytoplasm and nuclear accumulation of NF- κ B (Fig. S4A); however, CBAP did not influence the levels of PSPC1 and Pdx1 (Fig. S3). Also, we observed CBAP downregulates the expression of NOD2, which regulates the activity of NF- κ B (Fig. 5F). The molecular docking results suggested that similar to GSK717, a traditional inhibitor of NOD2, BA can also directly bind to NOD2 (Fig. 5G and H, Fig. S5), and the distance between BA and GLU-258 amino acid residues or SER-773 amino acid residues of NOD2 are listed in Tab.S1. This suggests that NOD2 and NF- κ B are involved in regulating the expression of ABC transporters. To verify this hypothesis, we downregulated NOD2 by GSK717. Inhibition of NOD2 impaired the total expression and nuclear accumulation of NF- κ B (Fig. 5I, Fig. S4B), and decreased the expression of ABC transporters (Fig. 5J). In addition, we observed that inhibition of NOD2 promotes GEM-induced apoptosis (Fig. 5K) but not influence pyroptosis (Fig. 5L). This suggested that CBAP increased chemosensitivity by targeting NOD2 and inhibiting NF-

κ B activity.

To evaluate whether CBAP regulated unclassified ABC transporters, we systematically treated the cells with CBAP and evaluated the expression of ABC transporters. We observed that CBAP significantly decreased the levels of CFTR (Fig. S6). To investigate how CBAP regulates the expression of CFTR, we evaluated the expression of NF- κ B and CTFR in MIA PaCa-2 cells and GEM-MIA PaCa-2 cells. Western blot analysis indicated that CBAP decreased the expression of CFTR by impairing the activity of NF- κ B (Fig. 6A). Indeed, downregulating the expression of NF- κ B decreased the levels of CFTR (Fig. 6B). In addition, Annexin V-APC and PI staining proved that inhibition of CFTR activity significantly increased GEM-mediated apoptosis (Fig. 6C). These results suggested that CFTR was also responsible for GEM resistance.

To evaluate how CFTR regulates the resistance of pancreatic cancer cells to GEM, we investigated autophagic flux, as we previously reported that blocking autophagy enhanced the anticarcinoma activity of GEM (Zhang et al., 2019b). Indeed, we observed that downregulating the expression of CFTR by PPQ-102 increased the accumulation of LC3II and p62 in the presence or absence of BAF1, an inhibitor of lysosomal degradation (Fig. 6D). The accumulation of autophagosomes was observed by TEM (Fig. 6E) and confocal microscopy (Fig. 6F). This suggested that PPQ-102 blocked autophagic flux, and similar results were obtained when cells were treated with CBAP (Fig. 6G and H). To verify whether blocking autophagy increased the sensitivity of cancer cells to GEM, we treated MIA PaCa-2 cells with 5 μM CQ and 10 μM GEM (Fig. 6I) and observed that CQ blocked autophagic flux and increased the accumulation of LC3 and p62. Moreover, blocking autophagy significantly enhanced the anticarcinoma activity of GEM (Fig. 6J). In conclusion, these data indicate that CBAP reverses the resistance of pancreatic cancer by targeting NOD2 and blocking autophagic flux.

4. Discussion

Although many studies have shown that BA inhibits the growth of a variety of tumors, including breast, lung, and pancreatic cancers, few studies have reported the organ toxicity of BA, especially cardiotoxicity, which prevents the drug from being clinically used (Sheng et al., 2021; Soumoy et al., 2022). In the present study, we observed that the IC_{50} of BA was lower than that of GEM in pancreatic cancer cells (Fig. S7, Fig. 1A and B). This suggests that the anticancer activity of BA is superior to that of GEM. However, it leads to severe toxicity. Even though we used a very low dosage (1 mg/kg BA) for intraperitoneal injection, we still observed that BA induced cardiotoxicity and significantly decreased the activity of mice (Fig. 1J-L).

CPN is a novel and promising strategy for the delivery of drugs. Compared to traditional delivery systems, CPNs are camouflaged by cell membrane vesicles, thereby allowing these nanoparticles to retain a high degree of similarity to their cancer target cells in terms of structure and function (Anaya-Ruiz et al., 2019; Fang et al., 2023). This also allows CPNs to escape clearance by mononuclear phagocytes (Wang et al., 2023). Currently, several cell membranes, such as erythrocytes, lymphocytes, platelets, and cancer cells, have been used to camouflage nanoparticles (Zeng et al., 2023). Compared to other membranes, cancer cell membranes are easy to obtain because of the proliferative capacity of cancer cells. In addition, cancer cell membranes exhibit unique homologous adhesion molecules that enhance tumor targeting (Wu et al., 2023). Therefore, to reduce cardiotoxicity and increase the accumulation of BA in tumor cells, we developed CBAP for the present study by using carcinoma cell membranes (Fig. 2A). We observed that 1 mg/kg CBAP did not lead to cardiotoxicity (Fig. 3L). Similar to BA, other digitalis analogs are also highly toxic. Their therapeutic dosages are very similar to toxic doses, which extremely narrows the safe range of dosages (Bauman et al., 2006). Cell membrane camouflaged technology is a promising strategy to solve this challenging problem. Future studies should investigate which kind of cell membrane is the optimal tool for the transport of BA and other digitalis analogs.

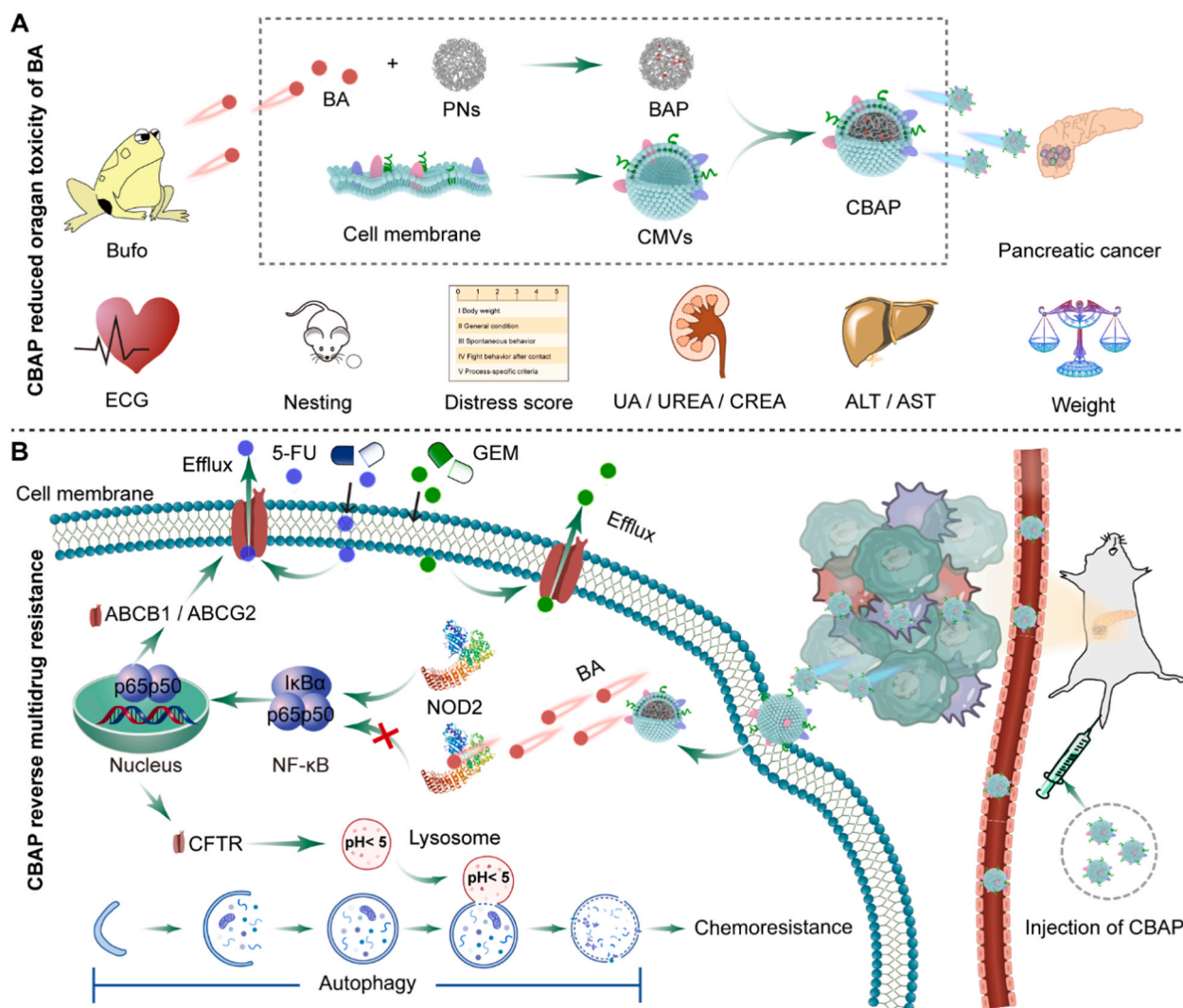


Fig. 7. CBAP effectively reduces the organ toxicity of BA and reverses multidrug resistance in pancreatic cancer. (A) We encapsulated BA in the cell membrane camouflaged PLGA nanoparticles to prepare CBAP, and CBAP did not impair the heart, liver and kidney of mice. (B) We found that CBAP targeted NOD2 directly and reversed chemoresistance via the NOD2/NF-κB/ABC transporter axis.

In the present study, CBAP significantly reversed the resistance of pancreatic cancer cells to first-line chemotherapeutics, such as GEM, by enhancing GEM-mediated apoptosis and pyroptosis (Fig. 5). This suggests that CBAP may be a promising strategy for the treatment of pancreatic cancer by targeting multiple molecules and inducing different forms of cell death. Previous studies proved that the ABC transporter family plays a vital role in the chemoresistance of pancreatic cancer (Capula et al., 2022; Gu et al., 2022). Totally 48 kinds of proteins in ABC transporter family have been identified; however, only some of them are involved in the efflux-mediated chemoresistance of pancreatic cancer cells (Bueschbell et al., 2022; Fan et al., 2023; Lu et al., 2019; Tanaka et al., 2011). For example, Dong et al. proved that ABC transporters, such as ABCB1, caused resistance of pancreatic cancer cells against GEM (Bai et al., 2022). Indeed, we observed that CBAP downregulates the expression of ABCB1 and ABCG2, and overcomes multidrug resistance by inhibiting the NOD2/NF-κB axis (Fig. 5). This result suggested that expressions of ABC transporters and NOD2 are proportional to the anticarcinoma activity of GEM.

To identify other ABC transporters that lead to chemotherapeutic drug resistance, we systematically evaluated the expression of ABC transporters by RNA sequencing and observed that CBAP significantly decreased the expression of CFTR. Mutations in *CFTR* have been identified as significant risk factors for developing pancreatic cancer (Malats

et al., 2001; McWilliams et al., 2010; Singh et al., 2007). Interestingly, we observed that CBAP inhibits the expression of CFTR and increases the sensitivity of pancreatic cancer cells to GEM. This suggests that CFTR may be involved in chemoresistance (Fig. 6). CFTR is a membrane protein responsible for the transmembrane transport of chloride and bicarbonate ions (Baharara et al., 2023). Intracellular bicarbonate ions and pH regulate autophagy and contribute to the response of cancer cells to chemical drugs. For example, SLC4A7, a member of the Na^+/H^+ exchanger family, is involved in the sensitivity of cancer cells to 56 drugs, such as mitomycin, spiromustine, and mitoxantrone (Huang et al., 2004; Li et al., 2022). Therefore, we evaluated the level of autophagy and observed that inhibition of CFTR blocked autophagic flux and increased the sensitivity of cancer cells to chemotherapy. This may be a result of increased intracellular pH and impairment of lysosomal function. Currently, some inhibitors of CFTR, such as PPQ-102 and CFTR-inh172, are being evaluated in the treatment of SARS-CoV-2 (Lagni et al., 2023) and T-cell acute lymphoblastic leukemia (Liu et al., 2019). To the best of our knowledge, no study has evaluated the benefit of CFTR inhibitors in treating pancreatic cancer and autophagy-associated diseases. Thus, future studies need to verify our observations.

Indeed, the present study proves that CBAP effectively reduces BA-mediated cardiotoxicity and overcomes multidrug resistance in

pancreatic cancer. However, there are still some limitations. First, we did not evaluate the purity of the cell membrane extract. Due to the malignant biological behavior of cancer cells, it is necessary to clear the nucleus and genes from the cell membranes and eliminate the carcinogenic risk. Thus, future studies need to investigate the risk of cell membrane-camouflaged nanoparticles in tumorigenesis. As mentioned before, several cell membranes, such as erythrocytes, lymphocytes, platelets and cancer cells, have been used to camouflage nanoparticles (Dhas et al., 2022). However, the current study does not investigate which kind of cell membrane is optimal to deliver BA as well as other digitalis analogs. Mechanistically, the present study indicates that CFTR is involved in the chemoresistance of pancreatic cancer cells. Furthermore, we also observed a slight elevation in the expression of CFTR in the GEM-resistant MIA PaCa-2 cells (GEM-MIA PaCa-2) compared to their parental counterparts (Fig. S8). However, how CFTR affects multidrug resistance still needs to be elucidated. In general, CFTR was reported to be expressed on the surface of lysosomal or cytoplasmic membranes, where it plays a crucial role in transporting chloride and bicarbonate ions (Baharara et al., 2023). Further elucidation is required to determine whether CFTR functions as a pump, akin to ABCB1 and ABCG2, facilitating drug efflux from cells and ultimately mediating chemoresistance. Clarifying this issue will further expand our understanding of CFTR and multidrug resistance.

5. Conclusion

In conclusion, the present study developed a novel nanodrug called CBAP, which effectively alleviates the cardiotoxicity associated with BA (Fig. 7A) and reverses the resistance of pancreatic cancer cells to GEM and 5-FU (Fig. 7B). The underlying mechanism involves direct binding to NOD2, leading to impaired NF- κ B activity. This inhibits the expression of the classic ABC transporters ABCB1 and ABCG2, which leads to the efflux of chemical drugs and contributes to pancreatic cancer chemoresistance (Fig. 7B). In addition, CBAP-mediated inhibition of NF- κ B decreases the expression of CFTR and hinders autophagic flux, another contributor to chemoresistance in pancreatic cancer (Fig. 7B). Thus, CBAP is a promising nanodrug that efficiently reverses drug resistance by targeting the NOD2/NF- κ B signaling pathway and regulating multiple mechanisms.

CRedit authorship contribution statement

XZ and PG conceived, designed and supervised this study. WZ, YF, JZ, JY and MA performed methodology, investigation and data collection. DS performed data analysis with RNA-seq and molecular docking. XZ, WZ and SF conducted validation and formal analysis. XZ, WZ, YC and PG wrote and revised the original manuscript. WL, MH, AMA, AH, ML and WGL contributed to design experiments and review the draft. XZ and WZ review and edit the final manuscript.

Declaration of Competing Interest

The authors declare that they have no known competing financial interests or personal relationships that could have appeared to influence the work reported in this paper.

Acknowledgments

This work was supported by the National Natural Science Foundation of China (82104596, 81973646), Guangdong Basic and Applied Basic Research Fund (2022A1515110832), China Postdoctoral Science Foundation (2022M722180), Shenzhen Key Medical Discipline Construction Fund & Sanming Project of Medicine in Shenzhen (SZSM202111002), Shenzhen Overseas High-Caliber Personnel Foundation and Shenzhen Science and Technology Program (GJHZ20220913143005010). We would also like to thank Shuyi Cai and

Chunhong Lian for their excellent Western blot technical assistance.

Appendix A. Supporting information

Supplementary data associated with this article can be found in the online version at doi:10.1016/j.drug.2023.101005.

References

- Anaya-Ruiz, M., Bandala, C., Landeta, G., Martínez-Morales, P., Zumaquero-Rios, J.L., Sarracent-Pérez, J., Pérez-Santos, M., 2019. Nanostructured systems in advanced drug targeting for the cancer treatment: recent patents. *Recent Pat. Anticancer Drug Discov.* 14, 85–94. <https://doi.org/10.2174/1574892813666181031154146>.
- Asrorov, A.M., Kayumov, M., Mukhamedov, N., Yashin, A., Mirakhmetova, Z., Huang, Y., Yili, A., Aisa, H.A., Tashmukhamedov, M., Salikhov, S., Mirzaakhmedov, S., 2023. Toad venom bufadienolides and bufotoxins: an updated review. *Drug Dev. Res.* <https://doi.org/10.1002/ddr.22072>.
- Ashrafzadeh, M., Delfi, M., Zarrabi, A., Bigham, A., Sharifi, E., Rabiee, N., Paiva-Santos, A.C., Kumar, A.P., Tan, S.C., Hushmandi, K., Ren, J., Zare, E.N., Makvandi, P., 2022. Stimuli-responsive liposomal nanoformulations in cancer therapy: pre-clinical & clinical approaches. *J. Control Release* 351, 50–80. <https://doi.org/10.1016/j.jconrel.2022.08.001>.
- Baharara, H., Kesharwani, P., Johnston, T.P., Sahebkar, A., 2023. Therapeutic potential of phytochemicals for cystic fibrosis. *BioFactors.* <https://doi.org/10.1002/biof.1960>.
- Bai, Z., Guo, Z., Liu, J., Chen, Y.A., Lu, Q., Zhang, P., Hong, L., Wang, Y., Dong, J., 2022. Lapatinib suppresses HER2-overexpressed cholangiocarcinoma and overcomes ABCB1-mediated gemcitabine chemoresistance. *Front Oncol.* 12, 860339 <https://doi.org/10.3389/fonc.2022.860339>.
- Bauman, J.L., DiDomenico, R.J., Galanter, W.L., 2006. Mechanisms, manifestations, and management of digoxin toxicity in the modern era. *Am. J. Cardiovasc. Drugs* 6, 77–86. <https://doi.org/10.2165/00129784-200606020-00002>.
- Bick, R.J., Poindexter, B.J., Sweney, R.R., Dasgupta, A., 2002. Effects of Chan Su, a traditional Chinese medicine, on the calcium transients of isolated cardiomyocytes: cardiotoxicity due to more than Na, K-ATPase blocking. *Life Sci.* 72, 699–709. [https://doi.org/10.1016/s0024-3205\(02\)02302-0](https://doi.org/10.1016/s0024-3205(02)02302-0).
- Bueschbell, B., Caniceiro, A.B., Suzano, P.M.S., Machuqueiro, M., Rosário-Ferreira, N., Moreira, I.S., 2022. Network biology and artificial intelligence drive the understanding of the multidrug resistance phenotype in cancer. *Drug Resist Updat* 60, 100811. <https://doi.org/10.1016/j.drug.2022.100811>.
- Capula, M., Perán, M., Xu, G., Donati, V., Yee, D., Gregori, A., Assaraf, Y.G., Giovannetti, E., Deng, D., 2022. Role of drug catabolism, modulation of oncogenic signaling and tumor microenvironment in microbe-mediated pancreatic cancer chemoresistance. *Drug Resist Updat* 64, 100864. <https://doi.org/10.1016/j.drug.2022.100864>.
- Chen, J., Wang, H., Jia, L., He, J., Li, Y., Liu, H., Wu, R., Qiu, Y., Zhan, Y., Yuan, Z., Cao, Y., Li, W., Xu, K., Yin, P., 2021. Bufalin targets the SRC-3/MIF pathway in chemoresistant cells to regulate M2 macrophage polarization in colorectal cancer. *Cancer Lett.* 513, 63–74. <https://doi.org/10.1016/j.canlet.2021.05.008>.
- Chen, S., Cheng, A.C., Wang, M.S., Peng, X., 2008. Detection of apoptosis induced by new type gosling viral enteritis virus *in vitro* through fluorescein annexin V-FITC/PI double labeling. *World J. Gastroenterol.* 14, 2174–2178. <https://doi.org/10.3748/wjg.14.2174>.
- Chen, Z., Zhao, P., Luo, Z., Zheng, M., Tian, H., Gong, P., Gao, G., Pan, H., Liu, L., Ma, A., Cui, H., Ma, Y., Cai, L., 2016. Cancer cell membrane-biomimetic nanoparticles for homologous-targeting dual-modal imaging and photothermal therapy. *ACS Nano* 10, 10049–10057. <https://doi.org/10.1021/acsnano.6b04695>.
- Cheng, C.S., Wang, J., Chen, J., Kuo, K.T., Tang, J., Gao, H., Chen, L., Chen, Z., Meng, Z., 2019. New therapeutic aspects of steroidal cardiac glycosides: the anticancer properties of Huachansu and its main active constituent Bufalin. *Cancer Cell Int.* 19, 92. <https://doi.org/10.1186/s12935-019-0806-1>.
- Deacon, R., 2012. Assessing burrowing, nest construction, and hoarding in mice. *J. Vis. Exp.*, e2607 <https://doi.org/10.3791/2607>.
- Dhas, N., García, M.C., Kudarha, R., Pandey, A., Nikam, A.N., Gopalan, D., Fernandes, G., Soman, S., Kulkarni, S., Seetharam, R.N., Tiwari, R., Wairkar, S., Pardeshi, C., Mutalik, S., 2022. Advancements in cell membrane camouflaged nanoparticles: a bioinspired platform for cancer therapy. *J. Control Release* 346, 71–97. <https://doi.org/10.1016/j.jconrel.2022.04.019>.
- Du, J., Zheng, L., Gao, P., Yang, H., Yang, W.-J., Guo, F., Liang, R., Feng, M., Wang, Z., Zhang, Z., 2022. A small-molecule cocktail promotes mammalian cardiomyocyte proliferation and heart regeneration. *e513 Cell Stem Cell* 29, 545–558. <https://doi.org/10.1016/j.stem.2022.03.009>.
- Duan, X., Li, Y., 2013. Physicochemical characteristics of nanoparticles affect circulation, biodistribution, cellular internalization, and trafficking. *Small* 9, 1521–1532. <https://doi.org/10.1002/smll.201201390>.
- El Amrani, M., Corfiotti, F., Corvaisier, M., Vasseur, R., Fulbert, M., Skrzypczyk, C., Deshorgues, A.C., Gnemmi, V., Tulasne, D., Lahdaoui, F., Vincent, A., Pruvot, F.R., Van Seuning, I., Huet, G., Truant, S., 2019. Gemcitabine-induced epithelial-mesenchymal transition-like changes sustain chemoresistance of pancreatic cancer cells of mesenchymal-like phenotype. *Mol. Carcinog.* 58, 1985–1997. <https://doi.org/10.1002/mc.23090>.
- Fan, J., To, K.K.W., Chen, Z.S., Fu, L., 2023. ABC transporters affects tumor immune microenvironment to regulate cancer immunotherapy and multidrug resistance. *Drug Resist Updat* 66, 100905. <https://doi.org/10.1016/j.drug.2022.100905>.

- Fang, R.H., Gao, W., Zhang, L., 2023. Targeting drugs to tumours using cell membrane-coated nanoparticles. *Nat. Rev. Clin. Oncol.* 20, 33–48. <https://doi.org/10.1038/s41571-022-00699-x>.
- Gu, J., Huang, W., Wang, X., Zhang, J., Tao, T., Zheng, Y., Liu, S., Yang, J., Chen, Z.S., Cai, C.Y., Li, J., Wang, H., Fan, Y., 2022. Hsa-miR-3178/RhoB/PI3K/Akt, a novel signaling pathway regulates ABC transporters to reverse gemcitabine resistance in pancreatic cancer. *Mol. Cancer* 21, 112. <https://doi.org/10.1186/s12943-022-01587-9>.
- Huang, X., Zhang, G., Tang, T.Y., Gao, X., Liang, T.B., 2022. Personalized pancreatic cancer therapy: from the perspective of mRNA vaccine. *Mil. Med Res* 9, 53. <https://doi.org/10.1186/s40779-022-00416-w>.
- Huang, Y., Anderle, P., Bussey, K.J., Barbacioru, C., Shankavaram, U., Dai, Z., Reinhold, W.C., Papp, A., Weinstein, J.N., Sadée, W., 2004. Membrane transporters and channels: role of the transportome in cancer chemosensitivity and chemoresistance. *Cancer Res* 64, 4294–4301. <https://doi.org/10.1158/0008-5472.Can-03-3884>.
- Iwamura, T., Katsuki, T., Ide, K., 1987. Establishment and characterization of a human pancreatic cancer cell line (SUIT-2) producing carcinoembryonic antigen and carbohydrate antigen 19-9. *Jpn J. Cancer Res* 78, 54–62.
- Jaster, R., Lichte, P., Fitzner, B., Brock, P., Glass, A., Karopka, T., Gierl, L., Koczan, D., Thiesen, H.J., Sparmann, G., Emmrich, J., Liebe, S., 2005. Peroxisome proliferator-activated receptor gamma overexpression inhibits pro-fibrogenic activities of immortalized rat pancreatic stellate cells. *J. Cell Mol. Med* 9, 670–682. <https://doi.org/10.1111/j.1582-4934.2005.tb00497.x>.
- Jiang, L., Tixeira, R., Caruso, S., Atkin-Smith, G.K., Baxter, A.A., Paone, S., Hulett, M.D., Poon, I.K., 2016. Monitoring the progression of cell death and the disassembly of dying cells by flow cytometry. *Nat. Protoc.* 11, 655–663. <https://doi.org/10.1038/nprot.2016.028>.
- Jin, Z.J., 1980. Addition in drug combination. *Zhongguo Yao Li Xue Bao* 1, 70–76.
- Koo, H., Huh, M.S., Sun, I.C., Yuk, S.H., Choi, K., Kim, K., Kwon, I.C., 2011. *In vivo* targeted delivery of nanoparticles for theranosis. *Acc. Chem. Res* 44, 1018–1028. <https://doi.org/10.1021/ar2000138>.
- Kumstel, S., Vasudevan, P., Palme, R., Zhang, X., Wendt, E.H.U., David, R., Vollmar, B., Zechner, D., 2020a. Benefits of non-invasive methods compared to telemetry for distress analysis in a murine model of pancreatic cancer. *J. Adv. Res.* 21, 35–47. <https://doi.org/10.1016/j.jare.2019.09.002>.
- Kumstel, S., Wendt, E.H.U., Eichberg, J., Talbot, S.R., Häger, C., Zhang, X., Abdelrahman, A., Schönrogge, M., Palme, R., Bleich, A., Vollmar, B., Zechner, D., 2020b. Grading animal distress and side effects of therapies. *Ann. N. Y. Acad. Sci.* 1473, 20–34. <https://doi.org/10.1111/nyas.14338>.
- Lagni, A., Lotti, V., Diani, E., Rossini, G., Concia, E., Sorio, C., Gibellini, D., 2023. CFTR inhibitors display *in vitro* antiviral activity against SARS-CoV-2. *Cells* 12. <https://doi.org/10.3390/cells12050776>.
- Li, C.X., Wang, J.S., Wang, W.N., Xu, D.K., Zhou, Y.T., Sun, F.Z., Li, Y.Q., Guo, F.Z., Ma, J.L., Zhang, X.Y., Chang, M.J., Xu, B.H., Ma, F., Qian, H.L., 2022. Expression dynamics of periodic transcripts during cancer cell cycle progression and their correlation with anticancer drug sensitivity. *Mil. Med Res* 9, 71. <https://doi.org/10.1186/s40779-022-00432-w>.
- Li, J., Zhu, L., Kwok, H.F., 2023. Nanotechnology-based approaches overcome lung cancer drug resistance through diagnosis and treatment. *Drug Resist. Updates* 66, 100904. <https://doi.org/10.1016/j.drug.2022.100904>.
- Liu, J., Li, S., Wang, J., Li, N., Zhou, J., Chen, H., 2022. Application of nano drug delivery system (NDDS) in cancer therapy: a perspective. *Recent Pat. Anticancer Drug Discov.* 18, 125–132. <https://doi.org/10.2174/1574892817666220713150521>.
- Liu, M., Liao, H., Chen, Y., Lin, Z., Liu, Y., Zhang, X., Chan, H.C., Sun, H., 2019. Treatment of human T-cell acute lymphoblastic leukemia cells with CFTR inhibitor CFTRinh-172. *Leuk. Res.* 86, 106225. <https://doi.org/10.1016/j.leukres.2019.106225>.
- Lopes, D., Lopes, J., Pereira-Silva, M., Peixoto, D., Rabiee, N., Veiga, F., Moradi, O., Guo, Z.H., Wang, X.D., Conde, J., Makvandi, P., Paiva-Santos, A.C., 2023. Bioengineered exosomal-membrane-camouflaged abiotic nanocarriers: neurodegenerative diseases, tissue engineering and regenerative medicine. *Mil. Med Res* 10, 19. <https://doi.org/10.1186/s40779-023-00453-z>.
- Lu, Y., Xu, D., Peng, J., Luo, Z., Chen, C., Chen, Y., Chen, H., Zheng, M., Yin, P., Wang, Z., 2019. HNF1A inhibition induces the resistance of pancreatic cancer cells to gemcitabine by targeting ABCB1. *EBioMedicine* 44, 403–418. <https://doi.org/10.1016/j.ebiom.2019.05.013>.
- Lu, Y., Gao, Y., Yang, H., Hu, Y., Li, X., 2022. Nanomedicine-boosting icaritin-based immunotherapy of advanced hepatocellular carcinoma. *Mil. Med. Res* 9, 69. <https://doi.org/10.1186/s40779-022-00433-9>.
- Malats, N., Casals, T., Porta, M., Guarnier, L., Estivill, X., Real, F.X., 2001. Cystic fibrosis transmembrane regulator (CFTR) DeltaF508 mutation and 5T allele in patients with chronic pancreatitis and exocrine pancreatic cancer. PANKRAS II Study Group. *Gut* 48, 70–74. <https://doi.org/10.1136/gut.48.1.70>.
- McWilliams, R.R., Petersen, G.M., Rabe, K.G., Holtegaard, L.M., Lynch, P.J., Bishop, M. D., Highsmith Jr., W.E., 2010. Cystic fibrosis transmembrane conductance regulator (CFTR) gene mutations and risk for pancreatic adenocarcinoma. *Cancer* 116, 203–209. <https://doi.org/10.1002/cncr.24697>.
- Miao, L., Liu, Y., Ali, N.M., Dong, Y., Zhang, B., Cui, X., 2023. Bufalin serves as a pharmaceutical that mitigates drug resistance. *Drug Metab. Rev.* 55, 195–204. <https://doi.org/10.1080/03602532.2023.2206065>.
- Nomoto, D., Baba, Y., Liu, Y., Tsutsuki, H., Okadome, K., Harada, K., Ishimoto, T., Iwatsuki, M., Iwagami, S., Miyamoto, Y., Yoshida, N., Watanabe, M., Moroiishi, T., Komohara, Y., Sawa, T., Baba, H., 2022. Fusobacterium nucleatum promotes esophageal squamous cell carcinoma progression via the NOD1/RIPK2/NF- κ B pathway. *Cancer Lett.* 530, 59–67. <https://doi.org/10.1016/j.canlet.2022.01.014>.
- Pacheco, C., Baião, A., Ding, T., Cui, W., Sarmento, B., 2023. Recent advances in long-acting drug delivery systems for anticancer drug. *Adv. Drug Deliv. Rev.* 194, 114724. <https://doi.org/10.1016/j.addr.2023.114724>.
- Sethy, C., Kundu, C.N., 2021. 5-Fluorouracil (5-FU) resistance and the new strategy to enhance the sensitivity against cancer: Implication of DNA repair inhibition. *Biomed. Pharm.* 137, 111285. <https://doi.org/10.1016/j.biopha.2021.111285>.
- Sheng, X., Zhu, P., Zhao, Y., Zhang, J., Li, H., Zhao, H., Qin, J., 2021. Effect of PI3K/AKT/mTOR signaling pathway on regulating and controlling the anti-invasion and metastasis of hepatoma cells by bufalin. *Recent Pat. Anticancer Drug Discov.* 16, 54–65. <https://doi.org/10.2174/1574892816666210201120324>.
- Siegel, R.L., Miller, K.D., Wagle, N.S., Jemal, A., 2023. Cancer statistics, 2023. *CA Cancer J. Clin.* 73, 17–48. <https://doi.org/10.3322/caac.21763>.
- Singh, A.P., Chauhan, S.C., Andrianifahanana, M., Moniaux, N., Meza, J.L., Copin, M.C., van Seuningen, I., Hollingsworth, M.A., Aubert, J.P., Batra, S.K., 2007. MUC4 expression is regulated by cystic fibrosis transmembrane conductance regulator in pancreatic adenocarcinoma cells via transcriptional and post-translational mechanisms. *Oncogene* 26, 30–41. <https://doi.org/10.1038/sj.onc.1209764>.
- Soumoy, L., Ghanem, G.E., Saussez, S., Journe, F., 2022. Bufalin for an innovative therapeutic approach against cancer. *Pharm. Res.* 184, 106442. <https://doi.org/10.1016/j.phrs.2022.106442>.
- Sparmann, G., Hohenadl, C., Tornøe, J., Jaster, R., Fitzner, B., Koczan, D., Thiesen, H.J., Glass, A., Winder, D., Liebe, S., Emmrich, J., 2004. Generation and characterization of immortalized rat pancreatic stellate cells. *Am. J. Physiol. Gastrointest. Liver Physiol.* 287, G211–G219. <https://doi.org/10.1152/ajpgi.00347.2003>.
- Tanaka, M., Okazaki, T., Suzuki, H., Abbruzzese, J.L., Li, D., 2011. Association of multi-drug resistance gene polymorphisms with pancreatic cancer outcome. *Cancer* 117, 744–751. <https://doi.org/10.1002/cncr.25510>.
- Valcourt, D.M., Harris, J., Riley, R.S., Dang, M., Wang, J., Day, E.S., 2018. Advances in targeted nanotherapeutics: from bioconjugation to biomimicry. *Nano Res* 11, 4999–5016. <https://doi.org/10.1007/s12274-018-2083-z>.
- Wang, J., Mao, W., Lock, L.L., Tang, J., Sui, M., Sun, W., Cui, H., Xu, D., Shen, Y., 2015. The role of micelle size in tumor accumulation, penetration, and treatment. *ACS Nano* 9, 7195–7206. <https://doi.org/10.1021/acsnano.5b02017>.
- Wang, J., Pan, H., Li, J., Nie, D., Zhuo, Y., Lv, Y., Wang, N., Chen, H., Guo, S., Gan, Y., Yang, X., Yu, M., 2023. Cell membrane-coated mesoporous silica nanorods overcome sequential drug delivery barriers against colorectal cancer. *Chin. Chem. Lett.* 34, 107828. <https://doi.org/10.1016/j.ccl.2022.107828>.
- Wu, L., Ge, Y., Yuan, Y., Li, H., Sun, H., Xu, C., Wang, Y., Zhao, T., Wang, X., Liu, J., Gao, S., Chang, A., Hao, J., Huang, C., 2022. Genome-wide CRISPR screen identifies MTA3 as an inducer of gemcitabine resistance in pancreatic ductal adenocarcinoma. *Cancer Lett.* 548, 215864. <https://doi.org/10.1016/j.canlet.2022.215864>.
- Wu, Y., Zhu, R., Zhou, M., Liu, J., Dong, K., Zhao, S., Cao, J., Wang, W., Sun, C., Wu, S., Wang, F., Shi, Y., Sun, Y., 2023. Homologous cancer cell membrane-camouflaged nanoparticles target drug delivery and enhance the chemotherapy efficacy of hepatocellular carcinoma. *Cancer Lett.* 558, 216106. <https://doi.org/10.1016/j.canlet.2023.216106>.
- Yan, R., Fan, X., Xiao, Z., Liu, H., Huang, X., Liu, J., Zhang, S., Yao, J., An, G., Ge, Y., 2022. Inhibition of DCLK1 sensitizes resistant lung adenocarcinomas to EGFR-TKI through suppression of Wnt/ β -Catenin activity and cancer stemness. *Cancer Lett.* 531, 83–97. <https://doi.org/10.1016/j.canlet.2022.01.030>.
- Zeng, S., Tang, Q., Xiao, M., Tong, X., Yang, T., Yin, D., Lei, L., Li, S., 2023. Cell membrane-coated nanomaterials for cancer therapy. *Mater. Today Bio* 20, 100633. <https://doi.org/10.1016/j.mtbio.2023.100633>.
- Zhan, Y., Qiu, Y., Wang, H., Wang, Z., Xu, J., Fan, G., Xu, J., Li, W., Cao, Y., Le, V.M., Ly, H.T., Yuan, Z., Xu, K., Yin, P., 2020. Bufalin reverses multidrug resistance by regulating stemness through the CD133/nuclear factor- κ B/MDR1 pathway in colorectal cancer. *Cancer Sci.* 111, 1619–1630. <https://doi.org/10.1111/cas.14345>.
- Zhang, D., Jia, T., Chen, X., Jiang, H., Guo, T., Dong, J., Zeng, H., Wang, Y., Yuan, Y., 2023. Bufalin reverses ABCB1-mediated resistance to docetaxel in breast cancer. *Heliyon* 9, e13840. <https://doi.org/10.1016/j.heliyon.2023.e13840>.
- Zhang, W., Yu, M., Xi, Z., Nie, D., Dai, Z., Wang, J., Qian, K., Weng, H., Gan, Y., Xu, L., 2019a. Cancer cell membrane-camouflaged nanorods with endoplasmic reticulum targeting for improved antitumor therapy. *ACS Appl. Mater. Interfaces* 11, 46614–46625. <https://doi.org/10.1021/acsmi.9b18388>.
- Zhang, W., Chen, L., Cui, M., Xie, L., Xi, Z., Wang, Y., Shen, X., Xu, L., 2021. Successively triggered Rod-shaped protocells for enhanced tumor Chemo-Photothermal therapy. *Eur. J. Pharm. Biopharm.* 169, 1–11. <https://doi.org/10.1016/j.ejpb.2021.08.012>.
- Zhang, X., Schönrogge, M., Eichberg, J., Wendt, E.H.U., Kumstel, S., Stenzel, J., Lindner, T., Jaster, R., Krause, B.J., Vollmar, B., Zechner, D., 2018. Blocking autophagy in cancer-associated fibroblasts supports chemotherapy of pancreatic cancer cells. *Front Oncol.* 8, 590. <https://doi.org/10.3389/fonc.2018.00590>.
- Zhang, X., Kumstel, S., Jiang, K., Meng, S., Gong, P., Vollmar, B., Zechner, D., 2019b. LW6 enhances chemosensitivity to gemcitabine and inhibits autophagic flux in pancreatic cancer. *J. Adv. Res.* 20, 9–21. <https://doi.org/10.1016/j.jare.2019.04.006>.
- Zhang, X., Kumstel, S., Tang, G., Talbot, S.R., Seume, N., Abshagen, K., Vollmar, B., Zechner, D., 2020a. A rational approach of early humane endpoint determination in a murine model for cholestasis. *Altx* 37, 197–207. <https://doi.org/10.14573/altex.1909111>.
- Zhang, X., Liu, P., Shang, Y., Kerndl, H., Kumstel, S., Gong, P., Vollmar, B., Zechner, D., 2020b. Metformin and LW6 impairs pancreatic cancer cells and reduces nuclear localization of YAP1. *J. Cancer* 11, 479–487. <https://doi.org/10.7150/jca.33029>.